Semi-Annual Report Submitted to the
National Aeronautics and Space Administration

For January - June, 2001

Contract Number: NAS5-31370

Land Surface Temperature Measurements from EOS MODIS Data

MODIS Team Member
PRINCIPAL INVESTIGATOR

ZHENGMING WAN

P.I.'s Address:

Institute for Computational Earth System Science
University of California
Santa Barbara, CA 93106-3060

phone : (805) 893-4541
Fax no: (805) 893-2578
E-mail: wan@icess.ucsb.edu

Land Surface Temperature Measurements from EOS MODIS Data

Semi-Annual Report for January - June, 2001

Zhengming Wan

This report presents the status of early Land-Surface Temperature (LST) at-launch standard product retrieved from Earth Observing System (EOS) Moderate Resolution Imaging Spectroradiometer (MODIS) data after a brief description of LST algorithms. Based on estimates of the channel-dependence error and noise equivalent temperature difference (NEDT) and the calibration accuracy of MODIS TIR data, the impact of instrument performance on the accuracy of LST is discussed. The accuracy of daily MODIS LST product at 1km resolution, which was produced by the generalized split-window algorithm, was validated with in-situ measurement data collected in field campaigns. The MODIS LST accuracy is better than 0.6K over Mono Lake, California, in three daytime and one nighttime cases, over a grassland in Bridgeport, California, in two nighttime cases, and over a rice field in Chico, California, in two nighttime cases. It is difficult to validate the daytime LST product over land sites rather than lakes with ground-based measurements alone because of the high spatial variations in the in-situ LST measurement data. One daytime flight of the MODIS Airborne Simulator (MAS) and the Airborne Visible Infrared Imaging Spectrometer (AVIRIS) and one nighttime MAS flight were conducted over sites in California in October 2000. The airborne data will be used to evaluate the MODIS LST product. Errors in the 1km LST product are expected to be larger in semi-arid and arid regions where surface emissivities in bands 31 and 32 are more variable. The MODIS LST product at 5km resolution generated by the day/night algorithm was released in beta version in late June 2001.

Recent Papers

Z. Wan, Estimate of noise and systematic error in early thermal infrared data of the Moderate Resolution Imaging Spectroradiometer (MODIS), *Remote Sens. Environ.,* in press 2001.

Z. Wan, Y. Zhang, Z.-L. Li, R. Wang, V.V. Salomonson, A. Yves, and R. Bosseno, Preliminary estimate of calibration of the Moderate Resolution Imaging Spectroradiometer (MODIS) thermal infrared data using Lake Titicaca, *Remote Sens. Environ.,* revised 2001.

X.-L. Ma, Z. Wan, C.C. Moeller, W.P. Menzel, and L.E. Gumley, Simultaneous retrieval of atmospheric profiles and land-surface temperature/emissivity from Moderate Resolution Imaging Spectroradiometer thermal infrared data: extension of a two-step physical algorithm, *IEEE Trans. Geosci. Remote Sens.,* submitted February 2001.

Z. Wan, Y. Zhang, R. Wang, and Z.-L. Li, Validation of the land-surface temperature product retrieved from Terra Moderate Resolution Imaging Spectroradiometer data, *Remote Sens. Environ.,* submitted March 2001.

1. Introduction

Remote sensing of sea surface temperature (SST) has been a primary function of satellite infrared radiometers since their inception, and starting from 1982 the SST derived from NOAA AVHRR (Advanced Very High Resolution Radiometer) data has been included in the high-resolution global SST climatology data set for global change studies (Brown et al., 1991; Smith and Reynolds, 1998). In comparison, there is no standard global LST data product derived from satellite remote sensing data even though the use of thermal-infrared measurements for analysis of land biophysical conditions has been under investigation for more than three decades (Fuchs and Tanner, 1966) and the AVHRR data have been used to produce regional LST data in the development of LST algorithms for two decades. It is well known that simple extension of the SST methods to LST for AVHRR data would lead to unacceptable errors (Price, 1984; Becker, 1987) because of the difficulty in cloud detection with AVHRR data (especially for thin cirrus) and the intrinsic difficulties in the LST retrieval (Wan and Dozier, 1989).

The MODIS (Salomonson et al., 1989) onboard the first EOS platform (called Terra), which was successfully launched on 18 December 1999, provides a new opportunity for global studies of atmosphere, land, and ocean processes (King et al., 1992; Justice et al., 1998; Esaias et al., 1998), and for satellite measurements of global LST. The strengths of MODIS include its global coverage, high radiometric resolution and dynamic ranges suitable for atmosphere, land, or ocean studies, and accurate calibration in multiple thermal infrared bands designed for retrievals of SST, LST and atmospheric properties. Specifically, band 26 will be used to detect cirrus clouds (Gao and Kaufman, 1995), band 21 for fire detection (Kaufman et al., 1998), all other TIR channels will be used to retrieve atmospheric temperature and water vapor profiles (Smith et al., 1985), and thermal infrared bands 20, 22, 23, 29, 31-33 will correct for atmospheric effects and retrieve surface emissivity and temperature (Wan and Li, 1997). This report will present the heritage of LST algorithms, the MODIS LST algorithms, a summary of early performance of MODIS TIR bands and its impact on the accuracy of retrieved LST, a brief description of the science data sets (SDS) in the MODIS LST product, early validation results, and a plan for the refinement of MODIS LST products and further validation in the following sections.

2. Heritage for LST Remote Sensing

A variety of LST methods have been published in the open literature. Here we provide some examples rather than a complete review. LST can be retrieved from a single infrared channel through an accurate radiative transfer model if surface emissivity is known and temperature/water vapor profile is given by either satellite soundings or conventional radiosonde data (Price, 1983; Susskind et al., 1984; Chedin et al., 1985; Ottlé and Vidal-Madjar, 1992). Split-window LST methods require known surface emissivities to make corrections for the atmospheric and surface emissivity effects based on the differential atmospheric absorption in the 10-13μm split window without knowledge of the atmospheric temperature/water vapor profile although column water vapor is used in some split-window LST algorithms to improve the accuracy of LST retrieval (Price, 1984; Becker, 1987; Wan and Dozier, 1989; Becker and Li, 1990; Sobrino et al., 1991; Vital, 1991; Kerr et al., 1992; Ottle and Stoll, 1993; Prata, 1994; Wan and Dozier, 1996). Because the accuracy of LST retrieved by single channel methods and split-window methods depends on the accuracy of surface emissivity, these methods do not work well in semi-arid and arid regions, where surface emissivity may vary significantly with location and time.

Methods which extract relative emissivities from multispectral thermal infrared data include reference channel method (Kahle et al., 1980), emissivity normalization method (Gillespie, 1985; Realmuto, 1990), TISI (temperature-independent spectral indices) method (Becker and Li, 1990), spectral ratio method (Watson, 1992), and alpha residuals method (Kealy and Gabell, 1990). Li et al. (1999) compares these methods with simulated TIMS (Thermal Infrared Multispectral Scanner) data, and shows that all these methods are sensitive to the uncertainties of atmosphere and an error of 20% in water vapor in mid-latitude summer atmosphere may lead to an error up to 0.03 in the relative emissivity in channel 1 of TIMS (at 8.379 μm), and the alpha method is even worser.

The TISI-based day/night method (Becker and Li, 1990) uses a pair of day/night co-registered AVHRR TIR data to estimate the bidirectional reflectance in channel 3, and then to estimate emissivity in this channel based on the Lambertian assumption of surface reflectance (Becker and Li, 1990) or a priori knowledge of bidirectional reflectance distribution function (BRDF) (Li and Becker, 1993), emissivities in channels 4 and 5 with TISI, and finally to estimate LST with the single channel method or the split-window method. If there are enough pairs of day/night co-registered AVHRR TIR data in a relative short period of time ranging from a few weeks to a few months depending on location and season in which surface BRDF does not change substantially and atmospheric temperature/water vapor profiles are available, directional emissivities at a series of view angles can be estimated using the integration of BRDF values in channel 3 estimated from AVHRR data (Nerry et al., 1998)

The temperature and emissivity separation algorithm for Advanced Spaceborne Thermal Emission and Reflection Radiometer (ASTER) (Gillespie et al., 1998) inherits features of the normalization method and spectral ratio method, and uses an empirical relationship of maximum-minimum emissivity difference (MMD) to refine estimates of surface emissivities and temperature.

In the above LST methods, only split-window methods do not require accurate atmospheric temperature/water vapor profile. Errors in emissivity and LST retrieved from all other method depends on uncertainties in the input atmospheric profile. It is well known that there are large spatial and temporal variations in atmospheric water vapor. Padilla et al. (1993) made psychrometric measurements for study of atmospheric humidity behavior at two places in Mexico, one in the Chaoultepec Heights, in the western zone of Mexico City at 2300m MSL, and another in Rancho Viejo, a mountainous wooded area at 2700m MSL. The distance between these places is approximately 68km. They found that the mixing ratio mean values for clear-sky days in the 1989 rainy season vary 30% in the period of 9:00-12:00 local time, 40% in

12:00-15:00. Bruegge et al. (1992) reported that water vapor column abundances retrieved from the Airborne Visible Infrared Imaging Spectrometer (AVIRIS) data during the First ISLSCP Field Experiment (FIFE) over the Konza Prairie, Kansas, on 31 August 1990, indicated that the spatial variability over scales associated with surface topography and the underlying vegetation may be greater than 10%.

Because of the close coupling between land surface and atmosphere, small changes in surface emissivities cause measurable changes in infrared radiances so that uncertainties in surface emissivities may result in large errors in the atmospheric temperature/water vapor retrieval (Plokhenko and Menzel, 2000). Therefore, we have to consider the potentially large uncertainties in the atmospheric temperature/water vapor profiles retrieved from satellite TIR data when we use the atmospheric profiles in the estimates of land-surface emissivity and temperature, especially in areas where surface emissivities are in low values and highly variable.

3. MODIS LST Algorithms

3.1. The Generalized Split-Window LST Algorithm

The LST of clear-sky pixels in MODIS scenes is retrieved with the split-window algorithm in a general form (Wan and Dozier, 1996)

$$T_s = C + \left(A_1 + A_2 \frac{1-\varepsilon}{\varepsilon} + A_3 \frac{\Delta\varepsilon}{\varepsilon^2}\right) \frac{T_{31} + T_{32}}{2} + \left(B_1 + B_2 \frac{1-\varepsilon}{\varepsilon} + B_3 \frac{\Delta\varepsilon}{\varepsilon^2}\right) \frac{T_{31} - T_{32}}{2} \quad , \qquad (1)$$

where $\varepsilon = 0.5\,(\varepsilon_{31} + \varepsilon_{32})$, and $\Delta\varepsilon = \varepsilon_{31} - \varepsilon_{32}$ are the mean and the difference of surface emissivities in MODIS bands 31 and 32. T_{31} and T_{32} are brightness temperatures in these two split-window bands. The coefficients C, A_i and B_i, $i = 1, 2, 3$ are given by interpolation on a set of multi-dimensional look-up tables (LUT). The LUTs were obtained by linear regression of the MODIS simulation data from radiative transfer calculations over wide ranges of surface and atmospheric conditions. Improvements for the generalized split-window LST algorithm incorporated in the establishment of the LUTs include: 1) view-angle dependence, 2) column water vapor dependence, and 3) dependence on the atmospheric lower boundary temperature. The view-angle dependence is kept in one dimension of LUTs for a set of viewing angles covering the whole MODIS swath so that LST can be retrieved at higher accuracies for pixels at both small and large viewing zenith angles, and at best accuracies for pixels at nadir and small view angles. The column water vapor dependence is kept in another dimension of LUTs for a set of overlapping intervals of column water vapor so that the information of water vapor provided in the MODIS atmospheric product is used as the most likely range of the water vapor rather than its exact value because the uncertainties in the atmospheric water vapor may be large. Similarly, the information of the atmospheric lower boundary temperature (T_{air}) provided in the MODIS atmospheric product is also used to improve the LST retrieval accuracy. The LST accuracy can be improved further by iterations with the information of difference between surface temperature T_s and T_{air}. In the initial retrieval, the unknown surface temperature could vary from -16 to 16K from the T_{air} value. In the first iteration, the coefficients in two sub-ranges of $T_s - T_{air}$ (one is -16 to +4.5K, another is -4.5 to 16K) can be selected according to the difference between the retrieved T_s and T_{air} values. In the second iteration, coefficients in four sub-ranges can be selected. They are -16 to -4.5K, -9.5 to 4.5K, -4.5 to 9.5K, and 4.5 to 16K, respectively.

The band emissivities, also called classification-based emissivities (Snyder, 1998), are estimated from land cover types in each MODIS pixel through TIR BRDF and emissivity modeling (Snyder and Wan, 1998). In the at-launch MODIS LST processing, the University of Maryland IGBP-type land-cover based on AVHRR data (Townshend et al., 1994) is used to provide global land cover information at 1km grids. Errors and uncertainties in the classification-based emissivities may be large in semi-arid and arid regions because of the large temporal and spatial variations in surface emissivities.

3.2. The MODIS Day/Night LST Algorithm

A physics-based day/night algorithm (Wan and Li, 1997) was developed to retrieve surface spectral emissivity and temperature at 5km resolution from a pair of daytime and nighttime MODIS data in seven TIR bands, i.e., bands 20, 22, 23, 29, and 31-33. The inputs to this algorithm includes the MODIS calibrated radiance product (MOD021KM), geolocation product (MOD03), atmospheric temperature and water vapor profile product (MOD07), and cloudmask product (MOD35). In our knowledge, this day/night algorithm is the first operational LST algorithm that has a capability to adjust the uncertainties in atmospheric temperature and water vapor profiles for a better retrieval of the surface emissivity and temperature. Because we use a pair of daytime and nighttime MODIS data in seven bands, we have 14 observations. In the day/night algorithm, there may be maximum 14 unknown variables. The minimal set of the surface variables includes 7 band emissivities, daytime and nighttime surface temperatures. There are only five unknowns left for atmospheric variables. Because of the close coupling between land surface and atmosphere, uncertainties in surface emissivities may result in large errors in the atmospheric temperature/water vapor retrieval (Plokhenko and Menzel, 2000). These errors could exist in the shape of the retrieved temperature/humidity profile, and in the values of atmospheric temperature at the surface level (T_a) and column water vapor (cwv). Atmospheric radiative transfer simulations show that the MODIS radiances in the above seven TIR bands are relatively less sensitive to changes in the shapes of temperature and water vapor profiles. Therefore, we set four atmospheric variables (T_a and cwv, for daytime and nighttime, respectively). Then there is only one unknown left for the anisotropic factor of the solar beam BRDF at the surface. This anisotropic factor is defined by the ratio of the surface-reflected solar beam at the view direction of the MODIS sensor to the radiance that would have resulted if the surface reflected isotropically (such a surface is called Lambertian surface),

$$\alpha = \frac{\pi f_r(\mu; \mu_0, \phi_0)}{r} \quad , \tag{2}$$

where r is reflectance of the assumed Lambertian surface. Bidirectional reflectance measurements of sands and soils (Snyder et al., 1997b) show that although there are quite strong spectral variations in surface reflectance for most terrestrial materials in the 3.5-4.2μm wavelength range, their BRDF anisotropic factor in this wavelength range has very small variations in the order of 2%. Therefore, we can use a single anisotropic factor for bands 20, 22, and 23. Besides we assume: 1) The surface emissivity changes with vegetation coverage and surface moisture content. However, it does not significantly change in several days unless rain and/or snow occurs during the short period of time - particularly for bare soils in arid and semi-arid environments, for which the surface of the ground is normally dry (Kerr et al., 1992). 2) Atmospheric radiative transfer simulations show that in clear-sky conditions the surface-reflected diffuse solar irradiance term is much smaller than the surface-reflected solar beam term in the thermal infrared range, and the surface-reflected atmospheric downward thermal irradiance term is smaller than surface thermal emission. So the Lambertian approximation of the surface reflection does not introduce significant error in the 3-14 μm thermal infrared region. Then we can link hemispherical directional reflectance $r(\theta)$ to directional emissivity $\varepsilon(\theta)$ by $r(\theta) = 1 - \varepsilon(\theta)$ according to Kirchhoff's law. Based on the above assumptions, the radiance measured in MODIS band j can be expressed as

$$L(j) = t_1(j)\,\varepsilon(j)\,\mathrm{B}_j(T_s) + L_a(j) + L_s(j) + \frac{1-\varepsilon(j)}{\pi}\,[t_2(j)\,\alpha\,\mu_0\,E_0(j) + t_3(j)\,E_d(j) + t_4(j)\,E_t(j)]\,, \qquad (3)$$

where all terms are band-averaged, $\varepsilon(j)$ is the surface emissivity, $\mathrm{B}_j(T_s)$ is the radiance emitted by a blackbody at surface temperature T_s, $L_a(j)$ is the thermal path radiance, $L_s(j)$ is the path radiance resulting from scattering of solar radiation, and $E_0(j)$ is the spectral solar irradiance incident on the top of the atmosphere (normal to the beam). $E_d(j)$ and $E_t(j)$ are the band-averaged solar diffuse irradiance and atmospheric downward thermal irradiance at surface. And $t_i(j)$, $i = 1, .., 4$ are the band effective transmission functions weighted by the band response function, the corresponding radiance, and irradiance terms. Note that we have neglected the in-band spectral variation of the surface emissivity in reducing a general integral equation into eq. (3), and have omitted symbols of view angle and solar angle for most terms in the above equation. On the right-hand side of this equation, $\varepsilon(j)$, α, and $\mathrm{B}_j(T_s)$ depend on surface properties and conditions. All other terms depend on atmospheric water vapor and temperature profiles, solar angle and viewing angle. These terms can be given by numerical simulations of atmospheric radiative transfer. The set of 14 nonlinear equations in the day/night algorithm is solved with the statistical regression method and the least-squares fit method (Wan and Li, 1997).

Considering the angular variation in surface emissivity, we separate the whole range of MODIS viewing zenith angle into sub-ranges, and use one emissivity in each of the sub-ranges. In the day/night LST processing, we will select a pair of clear-sky daytime and night MODIS observations at view angles in a same sub-range whenever it is possible. If there is no such a pair of day/night observations available in a reasonable short period of time but there is a pair of day/night observations in different sub-ranges of view angle, we will use this less favorite pair for surface emissivity and temperature retrieval and set a lower quality for the retrieved results. Sometimes we have to make a tradeoff between a favorite period of time and a favorite pair of view angles for temporal variations versus angular variations in surface emissivities. If the time difference between daytime and nighttime observations is too long, the chance for a large change in surface emissivity will be high. In the new product generation executive (PGE) code (version 3), the whole range of MODIS viewing zenith angle is separated into four sub-ranges (0° - 40°, 40° - 52°, 52° - 60°, 60° - 65°, respectively), instead of two sub-ranges in the earlier versions.

4. Early Performance of MODIS TIR Bands

The specification and estimated performance of the Terra MODIS TIR bands are shown in Table I. The channel-dependent noise and systematic error in MODIS TIR channel data were evaluated with early MODIS data over lake and ocean sites in clear-sky days acquired with the A-side of scan mirror and electronics before the end of October 2000 (Wan, 2001). In 14 cases of sub-area sites with a size of 10 lines by 16 pixels each line, where the brightness temperature in band 31 changes within ±0.1K, average and standard deviation values of brightness temperatures in ten channels (consisting a ten-element linear detector array) of 16 MODIS TIR bands show the channel-dependent noise and systematic errors. It is found that the ninth channel in bands 21 and 24, and the fourth channel in band 22 are too noisy to use, and that the specification of noise equivalent temperature difference (NEDT) is reached in all other channels of the 16 MODIS TIR bands. There are significant channel-dependent systematic errors in 1-3 channels in bands 22, 23, 25, 27-30. After correcting the channel-dependent systematic errors, the quality of the MODIS TIR data is significantly improved in bands 22-25, and 27-30, and the NEDT specification is reached or nearly reached in all bands as shown in column 5 of Table I.

The absolute radiometric accuracy of MODIS TIR channel data was evaluated with in-situ data collected in a vicarious calibration field campaign conducted in Lake Titicaca, Bolivia, during May 26 and June 17, 2000 (Wan et al., 2001). The comparison between MODIS TIR data produced by the new Level-1B code (version 2.5.4) and the band radiances calculated with atmospheric radiative transfer code MODTRAN4.0 (Berk et al., 1999) based on lake surface temperatures measured by five IR radiometers deployed in the high-elevation Lake Titicaca, and the atmospheric temperature and water vapor profiles measured by radiosondes launched on the lake-shore on 13 and 15 June 2000, calm clear-sky days, shows good agreements in bands 29, 31 and 32 (within an accuracy of 0.5%) in daytime overpass cases. Sensitivity analysis indicates that the changes in the measured atmospheric temperature and water vapor profiles result in negligible or small effects on the calculated radiances in bands 20-23, 29, and 31-33. Therefore, comparisons for these bands were made for cases when lake surface temperature measurements were available but no radiosonde data were available, and in sub-areas of 10 by 16 pixels where there was no in-situ measurement but MODIS brightness temperatures in band 31 vary within ±0.15K by using the validated band 31 to determine lake surface temperatures. These comparisons show that the specified absolute radiometric accuracies (10% for the fire band 21, 0.75% for band 20, 0.5% for bands 31 and 32, 1% for other TIR bands) are reached or nearly reached in MODIS bands 21, 29 and 31-33. Comparisons indicate a calibration bias 2-3% in bands 20, 22 and 23. Note that it is difficult to obtain a definitive estimate in bands 24-25, 27-28, and 34-36 because of the larger effects of the variations and uncertainties in atmospheric temperature and water vapor profiles. Column 6 in Table I shows the estimated values of calibration bias, which are averaged from sub-areas with viewing zenith angles smaller than 50° on June 13 and 15.

As shown in columns 5 and 6 of Table I, MODIS bands 31 and 32, which are used to retrieve LST with the generalized split-window algorithm, meet the NEDT specification. The effects of calibration bias in these two bands on the LST algorithm reflect in the average and the difference of brightness temperatures in these two bands, i.e., in 0.5 $(T_{31} + T_{32})$ and 0.5 $(T_{31} - T_{32})$. The effect of calibration bias in the first term is negligible. The effect in the second term is around 0.3K, introducing an error of 0.5K or slightly larger to the retrieved LST. Although this amount of error is too large for SST to meet its accuracy specification of 0.3-0.5K, it is considered marginal for LST to meet the 1K accuracy specification.

The estimated performance of bands 20, 22-23, 29, and 31-33, which are used in the MODIS day/night LST algorithm, shows that the NEDT specification is achieved in all these bands, calibration bias is small for longwave bands but is about 2-3% of the radiance (corresponding to an error in brightness temperature of ≤ 0.6 K) in the three mid-wave bands. The effects of calibration bias in mid-wave bands on the retrieved surface emissivity and temperature are being evaluated.

5. Science Data Sets in MODIS LST Products

The LST data products are produced as a series of seven products. The sequence begins as a swath (scene) at a nominal pixel spatial resolution of 1km at nadir and a nominal swath coverage of 2030 or 2040 lines (along track, about five minutes of MODIS scans) by 1354 pixels per line. A summarized listing of the sequence of products is given in Table II. Products in the Earth Observing System Data and Information System (EOSDIS) are labeled as Earth Science Data Type (ESDT), the ESDT label "shortname" is used to identify the LST data products. Except for the initial daily LST products, MOD11_L2, MOD11A1, and MOD11B1, each LST product in the sequence is built from the previous LST products. These LST products are identified, in part, by product levels in the EOSDIS which indicate what spatial and temporal processing has been applied to the data. The first product, MOD11_L2, is a LST product at 1km spatial resolution for a swath. This product is the result of the generalized split-window LST algorithm (Wan and Dozier, 1996). The second product, MOD11A1, is a tile of daily LST product at 1km spatial resolution. It is generated by mapping the pixels from the MOD11_L2 products for a day to the Earth locations on the integerized sinusoidal projection. The third product, MOD11B1, is a tile of daily LST and emissivities at 5km spatial resolution. It is generated by the day/night LST algorithm (Wan and Li, 1997). The fourth product, MOD11A2, is an eight-day LST product by averaging the MOD11A1 product in a period of eight days. The fifth product, MOD11C1, is a daily global LST product in a geographic projection. It is created by assembling the MOD11A1 and MOD11B1 daily tiles together and resampling the 1km cell and 5km cell observations to the 0.25° spatial resolution of the Climate Modeling Grid (CMG) cells. The sixth product, MOD11C2, is an eight-day composite of LST at the same resolution as MOD11C1. The seventh product, MOD11C3, is a monthly composite of LST at the same resolution as MOD11C2. The day/night LST algorithm needs a pair of daytime and nighttime L1B data in seven TIR bands, atmospheric temperature and water vapor profiles in the MODIS atmospheric product MOD07_L2. Because this algorithm depends on many input scientific data sets, the assessment and refinement of the day/night LST algorithm need a longer time. So the MOD11B1 product was released in late June 2001, and its downstream LST products (MOD11C1-3) will be released later.

The level 2 LST product, MOD11_L2, is generated using the MODIS sensor radiance data product (MOD021KM), the geolocation product (MOD03), the cloud mask product (MOD35_L2), the quarterly landcover (MOD12Q1), and snow product (MOD10_L2). For complete global coverage, a MOD11_L2 LST product would be generated for all swaths acquired in daytime and nighttime on the Earth including the polar regions. This MOD11_L2 LST product contains nine scientific data sets (SDSs): LST, QC, Error_LST, Emis_31, Emis_32, View_angle, View_time, Latitude, and Longitude, as shown in Table III. The first seven DSDs are for 1km pixels. The last two DSDs are coarse resolution (5 km) latitude and longitude data. Each set corresponds to a center pixel of a block of 5 by 5 pixels in the LST SDS. A mapping relationship of geolocation data to the first seven DSDs is specified in the global attribute StructMetadata.0. The mapping relationship was created by the HDF-EOS SDPTK toolkit during production. Geolocation data is mapped to the first seven DSDs data with an offset = 2 and increment = 5. The first element (0,0) in the geolocation SDSs corresponds to element (2,2) in LST SDS, then increments by 5 in the cross-track or along-track direction to map geolocation data to the LST SDS element. Because of the bowtie-shaped overlaps of scan lines by the edge of swath (Masuoka et al., 1998), 1km latitude and longitude positions for the LST SDS may be interpolated and extrapolated from the coarse resolution (5 km) latitude and longitude SDSs only within each scan (10 lines for the 1km resolution data). The accuracy of resulting 1km latitude and longitude positions is a few tenths of 1km in relative flat regions. The error may be up to a half km in mountain areas. Users who need accurate latitude and longitude positions of LST pixels should use the latitude and longitude data in the MODIS geolocation product MOD03. Note that the number 65535 in uint16 (unsigned 16-bit integer) may be shown as -1s in 16-bit integer by some software toolkits, for example, by ncdump in the HDF toolkit. The effective calibration formula for the LST SDS is LST = the SDS data in uint16 * 0.02, giving a value in the range of 150-1310.7K.

The QC SDS in the data product provides additional information on algorithm results for each pixel. The QC SDS 16-bit data are stored as bit flags in the SDS. This QC information can be extracted by reading the bits in the 16-bit unsigned integer. The purpose of the QC SDS is to give the user information on algorithm results for each pixel that can be viewed in a spatial context. The QC information tells if algorithm results were nominal, abnormal, or if other defined conditions were encountered for a pixel. The QC information should be used to help determine the usefulness of the LST data for a user's needs. The bit flags in the QC SDS are listed in Table IV. The 16 bits are used for eight flags, and bits 00-01 are used for Mandatory QA flags which is defined by the MODIS Land group: 00 stands for a pixel in which LST is produced in good quality, not necessary to examine more detailed QA bits; 01 for a pixel with LST produced in unreliable or unquantifiable quality, recommend examination of more detailed QA bits; 10 for a pixel not produced due to cloud effects (note that LST is produced only for pixels in clear-sky conditions at the 99% confidence); 11 for a pixel not produced primarily due to reasons other than cloud (for example, in ocean). Because there are two different situations (10 for a cloudy pixel and 11 for a pixel in ocean) in the Mandatory QA flags bits, in which a pixel has no LST value rather than a Fill Value in SDS LST, Fill Value 0 cannot be understood as the fill value for the whole QC SDS. It should be understood as the fill value for the other seven flags. This means that users should first check if Fill Value 0 is used in SDS LST. If it is true, SDS QC of the pixel only indicates that pixel is a cloudy pixel or ocean pixel in bits 00-01, other seven flags are given fill values. Only for pixels with non-zero values in SDS LST, the value in Mandatory QA flags may be 00 or 01 for good quality or not, the values in other seven flags represent meaningful information related to the LST quality (specifically, zero means best quality).

The daily level 3 LST product at 1km spatial resolution, MOD11A1, is a tile of daily LST product gridded in the Integerized Sinusoidal projection. A tile contains 1200 by 1200 grids in 1200 rows and 1200 columns. The exact grid size at 1km spatial resolution is 0.928km by 0.928km. The daily MOD11A1 LST product is constructed with the results in the MOD11_L2 products of a day through mapping the SDSs of all pixels in MOD11_L2 products onto grids in the integerized sinusoidal projection and averaging the values in each grid. The SDSs in the MOD11A1 product include LST_Day_1km, QC_Day, Day_view_time, Day_view_angl, LST_Night_1km, QC_Night, Night_view_time, Night_view_angl, Emis_31, Emis_32, Clear_day_cov, and Clear_night_cov. LST_Day_1km and LST_Night_1km are also stored as uint16 numbers with the same attributes as in SDS LST of the MOD11_L2 product. QC_Day and QC_Night are defined as 8-bit numbers. The bit flags in MOD11A1's QC SDS are listed in Table V. Similarly, the fill value 0 is used for the flags other than Mandatory QA flags in QC_Day and QC_Night, when fill value is given for LST_Day_1km and LST_Night_1km. When non-zero values are given for LST_Day_1km and LST_Night_1km, zero in the flags other than Mandatory QA flags in QC_Day and QC_Night means best quality.

The daily 5km level 3 LST product, MOD11B1, has SDSs similar to those in MOD11A1, including seven band emissivities, that are simultaneously retrieved along with the daytime and nighttime LST values. Two new SDSs (LST_Day_5km_Aggregated_from_1km and LST_Night_5km_Aggregated_from_1km) have been added to the MOD11B1 product to store the LST values aggregated from the LST_Day_1km and LST_Night_1km data in the MOD11A1 product so that they can be used as quick looks of the LST product in the MODIS Land Global Browse web page (http://modland.nascom.nasa.gov/browse).

6. Validation of the MODIS LST Product

The MODIS LST algorithms were validated with MAS data collected in several field campaigns since the field campaign conducted over a silt playa in Railroad Valley, Nevada, in June 1997 (Snyder et al., 1997a). According to the experience gained in our field campaigns, the major sources of uncertainties in the LST validation are the spatial variations in surface temperature and emissivity within a MAS or MODIS pixel. When these spatial variations are significantly large, it will not be possible to accurately measure the surface temperature at the scale of pixel size with ground-based instruments.

In order to validate the MODIS LST product, we conducted three field campaigns in California in 2000: early April in Mono Lake and Bridgeport grassland, late July in Mono Lake, Bridgeport grassland and a rice field in Chico, and early October in Mono Lake. We selected Mono Lake as our primary site for LST validation in the first year of MODIS LST production because of the following considerations. Because water surface emissivity can be accurately calculated from refractive index and surface temperature is often much more uniform in lakes than other land sites, lake surface radiometric temperature at a scale of 1km may be accurately measured by IR radiometers at multiple locations in most cases. We know that the uncertainty in surface emissivities in MODIS bands 31 and 32, and the residual error in LST after correcting the atmospheric effects with the split-window method are the only two major error sources in the level-2 1km MODIS LST product (MOD11_L2). We can reduce the emissivity-related error source to minimal with lakes as validation sites so that the residual error related to atmospheric corrections in the LST algorithm can be estimated by the difference between measured lake surface temperatures and the values in the MODIS LST product. If the surface temperature values in the MODIS LST product agree well with the measured lake surface temperatures in Mono Lake in different seasons, this will become evidence of the capability of the MODIS LST algorithm in atmospheric effect corrections. Once an estimate of the atmospheric-correction related residual error is obtained, we can apply this estimate to MODIS LST values in other locations, where it may be difficult or even impossible to make accurate in-situ measurements of surface temperatures at the 1km scale because of terrain and spatial variations in LST. In this way, we can indirectly validate the MODIS LST product in non-lake areas where the surface emissivities in bands 31 and 32 can also be well estimated from the land cover types and viewing angle, such as in vegetated areas. However, errors in the 1km LST product are expected to be larger in semi-arid and arid regions where surface emissivities in bands 31 and 32 are more variable. We selected Mono Lake as our primary LST validation site also because of the relative short distance between the site and the UCSB campus and the distance between the site and the aircraft base (Dryden Flight Research Center) for the MAS instrument so that we can arrange our field campaigns more flexibly and efficiently. We can drive to the site from Santa Barbara with all ground-based instruments in two vehicles in a single day. It is possible to fly daytime and nighttime MAS missions in a single day when it is in good weather conditions.

As shown in Fig. 1, Mono Lake has a relatively large open water area in its eastern portion, approximately 13km in the S-N direction and 9km in the E-W direction. This portion will be covered by around 100 MODIS pixels. The elevation of Mono Lake is 1945m above sea level.

We use infrared radiation pyrometers (model KT15) manufactured by Heitronics and purchased through Wintronics as IR radiometers with a filter in the spectral range 10-13 μm for the lake and land surface temperature measurements. The temperature measurement accuracy is specified as 0.5K in a wide temperature range from -50 to 150 °C. The IR radiometer is powered by a 24V battery. We store its measurement data with a stand-alone, voltage data logger from Onset Computer Corporation. The recorded voltage values are converted to temperature values in steps of 0.2K, giving a quantization error of 0.1K. Routine calibrations with a blackbody at temperatures from 0 to 50 °C indicate that the accuracy of the IR radiometer is better than 0.2K. During the deployment for lake surface temperature measurements, each IR radiometer was supported by a floating system (shown in Fig. 3 of Wan et al., 2001). The IR radiometer mounted on the floating system looked down at a height of 75cm above the water surface with instant-field-of-view (IFOV) of 32cm in diameter. The effect of water emissivity on measurements with the IR radiometer is 0.7K under dry atmospheric conditions according to the procedure based on measured atmospheric temperature/water vapor profile and the spectral response function of the IR radiometer (Wan et al., 2001).

On April 4, 2000, a clear-sky day, two IR-radiometer floating systems were deployed at two permanent buoys in the eastern portion of Mono Lake (buoys 4 and 5), and third one in the middle. The averaged value of lake surface kinetic temperatures measured by the three IR radiometers at the MODIS overpass time is 283.81K, as shown in column 4 in Table VI. Seven thermistors were also deployed along a nylon rope between these two buoys. Each of them was connected to a datalogger in a floating bottle which was attached to the rope. The thermistors were approximately 1cm beneath the water surface. One of the thermistor was deployed near buoy 4 so that we can get the difference between the water temperature measured by the thermistor and the water surface kinetic temperature measured by the IR radiometer at this buoy position. It was approximately 0.6K at the MODIS overpass time. We applied this value to all water temperatures measured by the thermistors to get the lake surface kinetic temperature values above the thermistor positions. The averaged value of these lake surface temperatures is 283.56K as shown in column 5. The standard deviation in the ten measured lake surface temperatures is 0.35K (in column 6), which represents the spatial variation in the lake surface temperature along the line from buoy 4 to buoy 5. We use the averaged surface temperature measured by the IR radiometers as the average in-situ measured lake surface temperature in this case (in column 7). The averaged values of the latitude and longitude positions for the three IR radiometers are given in column 2. We can get the surface temperature retrieved from MODIS data (labeled as MODIS T_s in column 8 of Table VI) by interpolating the LST values in the MODIS LST product at the four pixels mostly close to this averaged latitude and longitude position. The value in parentheses in column 8 is the standard deviation of the LST values in these four pixels. Note that we cannot apply the 4-pixel interpolation to the April 4 case of Mono Lake because buoys 4 and 5 are too close to Paoha island in the middle of the lake. Therefore, we shifted the averaged buoy position to the east by 1km in this case only. The difference between the MODIS T_s value and the averaged in-situ measured lake surface temperature is shown in the last column of Table VI. It is 0.2K in the first Mono Lake case (dated April 4).

The next two cases are also for Mono Lake in the July field campaign. On July 25, two IR radiometers were deployed at buoys 6 and 7, and one thermistor-datalogger bottle was deployed at buoy 6 position and three more were distributed between these two buoy positions. The IR radiometers were taken from the lake after the MODIS overpass time. But the thermistor-datalogger bottles were left in the water for several days. No IR radiometer was deployed at night of July 27 because there was no boat available at night. We used the water temperatures measured by the thermistors after applying the difference between temperatures measured by the thermistor and IR radiometer on July 25 to get the in-situ measured lake surface temperature at the time of MODIS nighttime overpass on July 27 under the assumption that this temperature difference does not significantly change with time. Actually, the temperature gradient at lake surface does change with sun angle, atmospheric and surface wind conditions. Therefore, we should give less weight for the July 27 night case because in this case the lake surface temperature was not directly measured by IR radiometers.

On October 6, four IR radiometers were deployed at buoys 6-9, all in the middle of the open water area. No thermistor was used on that day because of the good positions of the IR radiometers. As shown in the last column for the four cases of Mono Lake in the upper part of Table VI, the differences between LST values from the MODIS LST product and the in-situ measured LST values range from -0.1K to 0.2K. They are in the same level of the IR radiometer accuracy and the spatial variations in surface temperatures measured by IR radiometers and MODIS. In the worst case, the uncertainties related to IR radiometer, spatial variations in the in-situ measured temperatures and in MODIS measured temperatures are 0.2K, 0.38K, and 0.2K, respectively. The root sum square (RRS) of all these three uncertainties is 0.5K in the worst case. Therefore, we got the estimate of the residual error after atmospheric effect corrections in the MODIS LST product, which is less than 0.5K.

The same supporting structure used in the floating system for the IR radiometer was also used in the field campaign conducted in the Bridgeport grassland in early April 2000 just before the flood-irrigation started on 15 April, giving IFOV of 32cm in diameter on the grassland surface. Because there was no cattle and horse grazing on the grassland during the field campaign, we were allowed to deploy four IR radiometers in the middle of a grassland owned by Hunewill Circle H Ranch. The four IR radiometers were placed at the corners of a rectangular with a length of 50m each side with the hope that the measured surface temperatures can be compared to MAS data. Unfortunately, there was no MAS flight over the Mono Lake and Bridgeport area until October in 2000 because of technical and schedule problems. At the beginning, one IR radiometer was intentionally deployed at a location where soil surface was more wet than other locations. The differences in the surface temperatures measured by the IR radiometers were up to 7K in daytime data and 5K in nighttime data around the MODIS overpass time. After we moved the IR radiometers into an area where grass was more uniform and there is no obvious difference in the soil surface moisture conditions, the differences were still around 2.5K. Because of the large variation in measured surface temperatures, we can not use the in-situ measurement data collected over the grassland in April to validate or invalidate the MODIS LST product.

During the late July field campaign, the Bridgeport grassland was irrigated, and there were cattle and horses grazing in the field. Instead of using the plastic supporting systems for the IR radiometers in the field, we set two poles by the edge of a grassland and fixed one IR radiometer at the top of each pole. The IR radiometer viewed toward the grassland surface at approximately 3.5m above ground, with IFOV of 1.5m in diameter. On July 27 and 29 nights, two persons each carrying one IR radiometer walked forward and back along two almost parallel transects in the middle of a grassland under the clear-sky moon lights for more than one hour covering the MODIS nighttime overpass times. We averaged the measured surface temperatures along the transects and found that the averaged values are compatible to the values measured by the IR radiometers on the poles. But the in-situ data collected during daytimes (only the July 25 case is shown in Table VI) cannot be used for the validation of MODIS daytime LST product because of the large spatial variation in daytime LST. We can make an estimate for the effect of road surface temperature on the LST in a MODIS pixel. Suppose that the road surface temperature is 10K warmer than the grassland surface temperature and a 3.5-meter wide road passes across a MODIS pixel of 1km by 1km. The road amounts 0.35% of the MODIS pixel. An increase of 1K in the surface temperature raises the thermal infrared radiance by about 1.5% in the 10-13 μm spectral range, so a temperature difference of 10K raises the thermal infrared radiance by 15%. Multiplying the radiance difference 15% caused by the warmer road surface temperature with the proportion 0.35% gives an increase of 5.25% in the total radiance of one MODIS pixel. An increase of 5.25% in the total radiance corresponds to an increase of 3.5K in the surface temperature for a MODIS pixel. This number is quite close to the δT_s value in the last column of Table VI for the case of Bridgeport grassland on July 25. We can also explain the δT_s value -2.5K in the case of Bridgeport grassland on April 4, with -7K for the difference between road surface temperature and grassland surface temperature. This is a reasonable value because the grassland surface should be warmer than road during day before irrigation. The above values are used only for explaining why the in-situ measurement data in Bridgeport grassland during daytime cannot be used to validate or invalidate the MODIS LST product. It is not practical to measure the surface temperature or just the road surface temperature in a MODIS pixel with ground-based instruments alone. This example also show the great advantage of the thermal infrared remote sensing with MODIS in providing the global LST distribution at 1km resolution in clear-sky conditions.

During the late July field campaign, we also set one pole for an IR radiometer in the middle of a rice field in Chico, California, which is a test site used by Dr. Richard E. Plant, University of California at Davis. Because a series of rice fields in a size of approximately 50m by 50m each are distributed in the area, there are only narrow roads and irrigation canals between them, and there is no large difference between the surface temperatures over rice canopy and roads at night, we believe that the surface temperature measured by a single IR radiometer is still useful for the validation of nighttime MODIS LST product.

All the MODIS LST data used in the validation in this study are produced from MODIS L1B data reprocessed with its PGE code in version 2.5.4 except the October 6 case in which the version of L1B data is 2.4.3. There is no significant difference in the TIR band data of the L1B product in versions 2.4.3 and 2.5.4 (details are available in the version history file at the MODIS Calibration Support Team home page mcstweb.gsfc.nasa.gov/Home.html). From the temperature difference values in the last column of Table VI, we found that the MODIS LST accuracy is better than 0.6K over Mono Lake, California, in three daytime and one nighttime cases, over a grassland in Bridgeport, California, in two nighttime cases, and over a rice field in Chico, California, in two nighttime cases.

7. Plan of Future Activities

In the V1 and V2 MODIS LST processing, the land cover product (MOD12Q1), which was used as input to provide global land cover information at 1km grids for the estimate of band surface emissivities, was generated from AVHRR data in early 90s. In areas where the land cover has been significantly changed in the last several years, the estimated surface emissivities based on outdated land cover information may have large errors. Starting from the first consistent-year reprocessing of MODIS products (V3) in June 2001, the quarterly land-cover product generated from MODIS data (Borak and Strahler, 1999) is used in the MODIS LST production. We expect that the quality of the MODIS LST product generated by the split-window algorithm will improve with the change of input land-cover product from the one generated from old AVHRR data to the one generated from current MODIS data.

Because the MODIS cloud mask product (MOD35_L2) is used in the MODIS LST processing to decide for which MODIS pixels LST values will be produced or not produced. The LST is retrieved only for pixels in clear-sky conditions at 99% confidence. If a real clear-sky pixel is classified as a cloudy pixel (rather than 99% clear) in the MODIS cloud mask product, there will be no retrieved LST value given in the MOD11_L2 product and a fill value is given for the LST SDS in the product. We found this situation in arid regions and high-elevation scenes. Occasionally real cloudy pixels are classified as clear-sky pixels at the 99% confidence level in the MODIS cloud mask product. Then the retrieved LST values in the MODIS LST products will be contaminated by the cloud effects. The MODIS cloudmask team is working on these problems. The quality of MODIS LST products will be improved as these problems are resolved in the MODIS cloud mask product.

A significant progress has been recently made in the simultaneous retrieval of surface temperature/emissivity and atmospheric temperature/humidity profile by dealing with the close coupling between atmosphere and land surface with daytime and nighttime observations in more MODIS TIR bands (Ma et al., 2001). We will further the improvement and refinement of the day/night LST algorithm and optimize the code for a better computational efficiency. With the MODIS data collected from the EOS AM platform Terra and to be collected from the EOS PM platform (named Aqua) in the near future, the improved day/night LST algorithm will provide the 5km resolution LST products with better diurnal information at the global scale.

The MAS data collected in the October 2000 field campaign will be used to validate the MODIS LST product in Bridgeport, CA, after receiving the final radiometric calibrated MAS data. LST validation activities will be also conducted in some well selected sites in semi-arid and arid regions in 2001 and coming years.

Acknowledgment

This work was supported by EOS Program contract NAS5-31370 of the National Aeronautics and Space Administration. The author would like to thank Dr. Robert Jellison, University of California/Sierra Nevada Aquatic Research Lab., Dr. Richard E. Plant, University of California at Davis, Mr. Stan Hunewill and Jeff Hunewill, Hunewill Guest Ranch, Bridgeport, California, for their supports in the LST validation activities. The MODIS data were generated by the Goddard DAAC under supports of MODIS MCST and SDDT. The MODIS LST product was generated by the MODAPS under supports of MODIS SDDT, its routine quality assessment was performed by the LDOPE, and the LST product was distributed by the EDC DAAC.

REFERENCES

Becker, F., ‘‘The impact of spectral emissivity on the measurement of land surface temperature from a satellite,’’ *Int. J. Remote Sens.*, vol. 8, no. 10, pp. 1509-1522, 1987.

Becker, F. and Z.-L. Li, ‘‘Toward a local split window method over land surface,’’ *Int. J. Remote Sens.*, vol. 11, no. 3, pp. 369-393, 1990.

Berk, A., G. P. Anderson, L. S. Bernstein, P. K. Acharya, H. Dothe, M. W. Matthew, S. M. Adler-Golden, J. H. Chetwynd, Jr., S. C. Richtmeier, B. Pukall, C. L. Allred, L. S. Jeong, and M. L. Hoke, ‘‘MODTRAN4 radiative transfer modeling for atmospheric correction,’’ *Optical Spectroscopic Techniques and Instrumentation for Atmospheric and Space Research III*, vol. 3756, SPIE, 1999.

Borak, J. S. and A. H. Strahler, ‘‘Feature selection and land cover classification of a MODIS-like data set for a semiarid environment,’’ *Int. J. Remote Sens.*, vol. 20, pp. 919-938, 1999.

Brown, O. B., R. H. Evans, and P. Cornillon, ‘‘Satellite-derived global sea surface temperature fields: 1982-1989,’’ *Global and Planetary Change*, vol. 90, pp. 179-181, 1991.

Bruegge, C. J., J. E. Conel, R. O. Green, J. S. Margolis, R. G. Holm, and G. Toon, ‘‘Water vapor column abundance retrievals during FIFE,’’ *J. Geophys. Res.*, vol. 97, no. D17, pp. 18759-18768, 1992.

Chedin, A., M. A. Scott, C. Wahiche, and P. Moulinier, ‘‘The improved initialization inversion method: a high resolution physical method for temperature retrievals from the Trios-N series,’’ *J. Clim. Appl. Meteorol.*, vol. 24, pp. 124-143, 1985.

Esaias, W. E., M. R. Abbott, I. Barton, O. W. Brown, J. W. Campbell, K. L. Carder, D. K. Clark, R. L. Evans, F. E. Hoge, H. R. Gordon, W. P. Balch, R. Letelier, and P. J. Minnett, ‘‘An overview of MODIS capabilities for ocean science observations,’’ *IEEE Trans. Geosci. Remote Sens.*, vol. 36, no. 4, pp. 1250-1265, 1998.

Fuchs, M. and C. B. Tanner, ‘‘Infrared thermometry of vegetation,’’ *Agron. J.*, vol. 58, pp. 597-601, 1966.

Gao, B. C. and Y. J. Kaufman, ‘‘Selection of the 1.375μm MODIS channel for remote sensing of cirrus cloud and stratospheric aerosols from space,’’ *J. Atmos. Sci.*, vol. 52, no. 23, pp. 4231-4237, 1995.

Gillespie, A., ‘‘Lithologic mapping of silicate rocks using TIMS,’’ in *TIMS Data Users’ Workshop*, pp. 29-44, Pasadena, CA: Jet Propul. Lab., JPL Publication 86-38, 1985.

Gillespie, A. R., S. Rokugawa, T. Matsunaga, J. S. Cothern, S. Hook, and A. B. Kahle, ‘‘A temperature and emissivity separation algorithm for Advanced Spaceborne Thermal Emission and Reflection Radiometer (ASTER) images,’’ *IEEE Trans. Geosci. Remote Sens.*, vol. 36, pp. 1113-1126, 1998.

Justice, C. O., E. Vermote, J. R. G. Townshend, R. Defries, D. O. Roy, D. K. Hall, V. V. Salomonson, J. L. Privette, G. Riggs, A. Strahler, W. Lucht, R. B. Myneni, K. Knyazikhin, S. W. Running, P. R. Nemani, Z. Wan, A. R. Huete, W. van Leeuwen, R. E. Wolfe, L. Giglio, J.-P. Muller, and Y. Knyazikhin, M. J. Barnsley, ‘‘The Moderate Resolution Imaging Spectroradiometer (MODIS): land remote sensing for global change research,’’ *IEEE Trans. Geosci. Remote Sens.*, vol. 36, pp. 1228-1249, 1998.

Kahle, A. B., D. P. Madura, and J. M. Soha, ‘‘Middle infrared multispectral aircraft scanner data: analysis for geological applications,,’’ *Appl. Optics*, vol. 19, pp. 2279-2290, 1980.

Kaufman, Y. J., C. O. Justice, L. P. Flynn, L. D. Kendall, E. M. Prins, L. Giglo, D. E. Ward, W. P. Menzel, and A. W. Setzer, ‘‘Potential global fire monitoring from EOS-MODIS,’’ *J. Geophys. Res.*, vol. 103, no. D24, pp. 32215-32238, 1998.

Kealy, P. S. and A. R. Gabell, ‘‘Estimation of emissivity and temperature using alpha coefficients,’’ in *Proc. 2nd TIMS Workshop*, pp. 11-15, Pasadena, CA: Jet Propul. Lab., JPL Publication 90-55, 1990.

Kerr, Y. H., J. P. Lagouarde, and J. Imbernon, ‘‘Accurate land surface temperature retrieval from AVHRR data with use of an improved split window algorithm,’’ *Remote Sens. Environ.*, vol. 41, no. 2-3, pp. 197-209, 1992.

King, M. D., Y. J. Kaufman, W. P. Menzel, and D. Tanré, ‘‘Remote sensing of cloud, aerosol, and water vapor properties from the Moderate Resolution Imaging Spectrometer (MODIS),’’ *IEEE Trans. Geosci. Remote Sens.*, vol. 30, no. 1, pp. 2-27, 1992.

Li, Z.-L. and F. Becker, ‘‘Feasibility of land surface temperature and emissivity determination from AVHRR data,’’ *Remote Sens. Environ.*, vol. 43, pp. 67-85, 1993.

Li, Z.-L., F. Becker, M. P. Stoll, and Z. Wan, ‘‘Evaluation of six methods for extracting relative emissivity spectra from thermal infrared images,’’ *Remote Sens. Environ.*, vol. 69, pp. 197-214, 1999.

Ma, X.-L., Z. Wan, C. C. Moeller, W. P. Menzel, and L. E. Gumley, ‘‘Simultaneous retrieval of atmospheric profiles and land-surface temperature/emissivity from Moderate Resolution Imaging Spectroradiometer thermal infrared data: extension of a two-step physical algorithm,’’ *IEEE Trans. Geosci. Remote Sens.*, submitted 2001.

Masuoka, E., A. Fleig, R. E. Wolfe, and F. Patt, ‘‘Key characteristics of MODIS data products,’’ *IEEE Trans. Geosci. Remote Sens.*, vol. 36, no. 4, pp. 1313-1323, 1998.

Nerry, F., F. Petitcolin, and M. P. Stoll, ‘‘Bidirectional reflectivity in AVHRR channel 3: application to a region in Northern Africa,’’ *Remote Sens. Environ.*, vol. 66, pp. 298-316, 1998.

Ottlé, C. and M. Stoll, ‘‘Effect of atmospheric absorption and surface emissivity on the determination of land temperature from infrared satellite data,’’ *Int. J. Remote Sens.*, vol. 14, no. 10, pp. 2025-2037, 1993.

Ottlé, C. and D. Vidal-Madjar, ‘‘Estimation of land surface temperature with NOAA9 data,’’ *Remote Sens. Environ.*, vol. 40, no. 1, pp. 27-41, 1992.

Padilla, H. G., A. C. Leyva, and P. A. Mosino, ‘‘An analysis of daily humidity patterns at a mountainous and urban site in a tropical high-altitude region,’’ *J. Appl. Meteorol.*, vol. 32, pp. 1638-1646, 1993.

Plokhenko, Y. and W. P. Menzel, ‘‘The effects of surface reflection on estimating the vertical temperature-humidity distribution from spectral infrared measurements,’’ *J. Appl. Meteorol.*, vol. 39, pp. 3-14, 2000.

Prata, A. J., ''Land surface temperatures derived from the advanced very high resolution radiometer and the along-track scanning radiometer 2. experimental results and validation of AVHRR algorithms,'' *J. Geophys. Res.*, vol. 99, no. D6, pp. 13025-13058, 1994.

Price, J. C., ''Estimating surface temperature from satellite thermal infrared data - a simple formulation for the atmospheric effect,'' *Remote Sens. Environ.*, vol. 13, pp. 353-361, 1983.

Price, J. C., ''Land surface temperature measurements from the split window channels of the NOAA-7 AVHRR,'' *J. Geophys. Res.*, vol. 79, pp. 5039-5044, 1984.

Realmuto, V. J., ''Separating the effects of temperature and emissivity: emissivity spectrum normalization,'' in *Proc. 2nd TIMS Workshop*, pp. 23-27, Pasadena, CA: Jet Propul. Lab., JPL Publication 90-55, 1990.

Salomonson, V., W. Barnes, P. Maymon, H. Montgomery, and H. Ostrow, ''MODIS: advanced facility instrument for studies of the Earth as a system,'' *IEEE Trans. Geosci. Remote Sens.*, vol. 27, no. 2, pp. 145-153, 1989.

Smith, T. M. and R. W. Reynolds, ''A high-resolution global sea surface temperature climatology for the 1961-90 base period,'' *J. Climate*, vol. 11, pp. 3320-3323, 1998.

Smith, W. L., H. M. Woolf, and A. J. Schriener, ''Simultaneous retrieval of surface and atmospheric parameters: a physical and analytically direct approach,'' in *Advances in Remote Sensing Retrieval Methods*, ed. A. Deepak, H. E. Fleming, and M. T. Chahine, pp. 221-232, Hampton, Va., USA: A. Deepak Publishing, 1985.

Snyder, W. and Z. Wan, ''BRDF models to predict spectral reflectance and emissivity in the thermal infrared,'' *IEEE Trans. Geosci. Remote Sens.*, vol. 36, no. 1, pp. 214-225, 1998.

Snyder, W., Z. Wan, Y. Zhang, and Y.-Z. Feng, ''Requirements for satellite land surface temperature validation using a silt playa,'' *Remote Sens. Environ.*, vol. 61, no. 2, pp. 279-289, 1997a.

Snyder, W., Z. Wan, Y. Zhang, and Y.-Z. Feng, ''Thermal infrared (3-14 μm) bidirectional reflectance measurements of sands and soils,'' *Remote Sens. Environ.*, vol. 60, pp. 101-109, 1997b.

Snyder, W. C., Z. Wan, Y. Zhang, and Y.-Z. Feng, ''Classification-based emissivity for land surface temperature measurement from space,'' *Int. J. Remote Sens.*, vol. 19, no. 14, pp. 2753-2774, 1998.

Sobrino, J. A., C. Coll, and V. Caselles, ''Atmospheric corrections for land surface temperature using AVHRR channel 4 and 5,'' *Remote Sens. Environ.*, vol. 38, no. 1, pp. 19-34, 1991.

Susskind, J., J. Rosenfield, D. Reuter, and M. T. Chahine, ''Remote Sensing of weather and climate parameters from HIRS2/MSU on TIROS-N,'' *J. Geophys. Res.*, vol. 89, no. D3, pp. 4677-4697, 1984.

Townshend, J. R. G., C. O. Justice, D. Skole, J.-P. Malingreau, J. Cihlar, P. Teillet, and S. Ruthenberg, ''The 1km resolution global data set: needs of the International Geosphere Biosphere Programme,'' *Int. J. Remote Sens.*, vol. 15, pp. 3417-3441, 1994.

Vidal, A., ''Atmospheric and emissivity correction of land surface temperature measured from satellite using ground measurements or satellite data,'' *Int. J. Remote Sens.*, vol. 12, no. 12, pp. 2449-2460, 1991.

Wan, Z. and J. Dozier, ‘‘A generalized split-window algorithm for retrieving land-surface temperature from space,’’ *IEEE Trans. Geosci. Remote Sens.*, vol. 34, no. 4, pp. 892-905, 1996.

Wan, Z. and J. Dozier, ‘‘Land-surface temperature measurement from space: physical principles and inverse modeling,’’ *IEEE Trans. Geosci. Remote Sens.*, vol. 27, no. 3, pp. 268-278, 1989.

Wan, Z., ‘‘Estimate of noise and systematic error in early thermal infrared data of the Moderate Resolution Imaging Spectroradiometer (MODIS),’’ *Remote Sens. Environ.*, in press 2001.

Wan, Z. and Z.-L. Li, ‘‘A physics-based algorithm for retrieving land-surface emissivity and temperature from EOS/MODIS data,’’ *IEEE Trans. Geosci. Remote Sens.*, vol. 35, no. 4, pp. 980-996, 1997.

Wan, Z., Y. Zhang, Z.-L. Li, R. Wang, V. V. Salomonson, A. Yves, and R. Bosseno, ‘‘Preliminary estimate of calibration of the Moderate Resolution Imaging Spectroradiometer (MODIS) thermal infrared data using Lake Titicaca,’’ *Remote Sens. Environ.*, revised 2001.

Watson, K., ‘‘Spectral ratio method for measuring emissivity,’’ *Remote Sens. Environ.*, vol. 42, pp. 113-116, 1992.

TABLE I. Specifications and estimated performance of the Terra MODIS TIR bands.

(1) band	(2) bandwidth (μm)	(3) IFOV	(4) NEDT specified (K)	(5) NEDT (K) estimated (Wan, 2001)	(6) calibration bias estimated (K) (Wan et al., 2001)	(7) primary use*
20	3.660-3.840	1km	0.05	0.06	0.61	O, L
21	3.929-3.989	1km	2.00	0.64	0.46	fire, volcano
22	3.929-3.989	1km	0.07	0.07	0.55	A, L
23	4.020-4.080	1km	0.07	0.05	0.40	A, L
24	4.433-4.498	1km	0.25	0.13		A
25	4.482-4.549	1km	0.25	0.08		A
27	6.535-6.895	1km	0.25	0.12		A
28	7.175-7.475	1km	0.25	0.09		A
29	8.400-8.700	1km	0.05	0.03	0.02	L
30	9.580-9.880	1km	0.25	0.08		ozone
31	10.780-11.280	1km	0.05	0.03	0.12	A, L
32	11.770-12.270	1km	0.05	0.05	-0.19	A, L
33	13.185-13.485	1km	0.25	0.16	0.55	A, L
34	13.485-13.785	1km	0.25	0.27		A
35	13.785-14.085	1km	0.25	0.23		A
36	14.085-14.385	1km	0.35	0.41		A

*Note: A - atmospheric studies, L - land studies, O - ocean studies.

TABLE II. A list of the MODIS LST data products.

Earth Science Data Type (ESDT)	Product Level	Nominal Data Array Dimension	Spatial Resolution	Temporal Resolution	Map Projection
MOD11_L2	L2	2030 or 2040 lines by 1354 pixels	1km at nadir	swath (scene)	none (lat, lon referenced)
MOD11A1	L3	1200 rows by 1200 columns	1km (actual 0.928km)	day	Integerized Sinusoidal
MOD11B1	L3	240 rows by 240 columns	5km (actual 4.638km)	day	Integerized Sinusoidal
MOD11A2	L3	1200 rows by 1200 columns	1km (actual 0.928km)	eight days	Integerized Sinusoidal
MOD11C1	L3	360° by 180° (global)	0.25° by 0.25°	day	Geographic
MOD11C2	L3	360° by 180° (global)	0.25° by 0.25°	eight days	Geographic
MOD11C3	L3	360° by 180° (global)	0.25° by 0.25°	month	Geographic

TABLE III. The SDSs in the MOD11_L2 product.

SDS Name	Long Name	Number Type	Unit	Valid Range	Fill Value	scale factor	add offset
LST	Land-surface temperature	uint16	K	7500-65535	0	0.02	0.
QC	Quality control for LST and emissivity	uint8	none	0-255	0	NA	NA
Error_LST	Land-surface temperature error	uint8	K	1-255	0	0.04	0.
Emis_31	Band 31 emissivity	uint8	none	1-255	0	0.002	0.49
Emis_32	Band 32 emissivity	uint8	none	1-255	0	0.002	0.49
View_angle	zenith angle of MODIS viewing at the pixel	uint8	deg.	0-180	0	0.5	0.
View_time	Time (local solar time) of Land-surface temperature observation	uint8	hrs	0-240	0	0.1	0.
Latitude	Latitude of every 5 scan lines and 5 pixels	float32	degree	-90.0 to 90.0	-999.9	NA	NA
Longitude	Longitude of every 5 scan lines and 5 pixels	float32	degree	-180.0 to 180.0	-999.9	NA	NA

TABLE IV. Bit flags defined in the QC SDS in the MOD11_L2 product.

bit	Long Name	Key
00-01	Mandatory QA flags	00 = Pixel produced, good quality, not necessary to examine more detailed QA 01 = Pixel produced, unreliable or unquantifiable quality, recommend examination of more detailed QA 10 = Pixel not produced due to cloud effects 11 = Pixel not produced primarily due to reasons other than cloud
02-03	Data quality flag	00 = good 01 = missing pixel 10 = fairly calibrated 11 = poorly calibrated, LST processing skipped
04-05	Cloud flag	00 = cloud free pixel 01 = pixel only with thin cirrus 10 = fraction of sub-pixel clouds<= 2/16 11 = TBD
06-07	LST model number	00 = generalized split-window method 01 = day/night method 10 = high LST w/o atmospheric & emis corrections 11 = cirrus effects corrected
08-09	LST quality flag	00 = no multi-method comparison 01 = multi-method comparison done 10 = fair consistency 11 = good consistency
10-11	Emissivity flag	00 = inferred from land cover type 01 = MODIS retrieved 10 = TBD 11 = default value used
12-13	Emissivity quality flag	00 = emis quality not checked 01 = emis quality checked with land cover type 10 = emis quality checked with NDVI 11 = emis view-angle dependence checked
14-15	Emissivity error flag	00 = error in emis_31 emis_32 <= 0.01 01 = error in emis_31 emis_32 <= 0.02 10 = error in emis_31 emis_32 <= 0.04 11 = error in emis_31 emis_32 > 0.04

TABLE V. Bit flags defined for SDS QC_Day and QC_Night in the MOD11A1 product.

bit	Long Name	Key
00-01	Mandatory QA flags	00 = Pixel produced, good quality, not necessary to examine more detailed QA 01 = Pixel produced, unreliable or unquantifiable quality, recommend examination of more detailed QA 10 = Pixel not produced due to cloud effects 11 = Pixel not produced primarily due to reasons other than cloud
02-03	Data quality flag	00 = good data quality 01 = LST affected by thin cirrus and/or sub-pixel clouds 10 = not processed due to missing pixels 11 = not processed due to poor quality
04-05	Emissivity error flag	00 = average emissivity error <= 0.01 01 = average emissivity error <= 0.02 10 = average emissivity error <= 0.04 11 = average emissivity error > 0.04
06-07	LST error flag	00 = average LST error <= 1K 01 = average LST error <= 2K 10 = average LST error <= 3K 11 = average LST error > 3K

TABLE VI. Comparison between MODIS LSTs and in-situ measured LSTs in validation field campaigns conducted in 2000.

(1) site	(2) latitude / longitude (°)	(3) date (m/d/y) time	(4) T_s from radiometers (K) (no.)	(5) T_s from thermistors (K) (no.)	(6) spatial δT_s (K)	(7) average in-situ T_s (K)	(8) MODIS T_s (δT_s) (K)	(9) δT_s (K)
Mono Lake	37.9712N / 119.0014W	4/04/00 11:19 PST	283.81 (3)	283.56 (7)	0.35	283.8	284.0 (0.2)	+0.2
Mono Lake	37.9930N / 118.9646W	7/25/00 11:18 PST	296.11 (2)	296.03 (4)	0.38	296.1	296.3 (0.2)	+0.2
Mono Lake	37.9930N / 118.9646W	7/27/00 23:09 PST		293.46 (4)	0.10	293.5	293.4 (0.1)	-0.1
Mono Lake	38.0105N / 118.9695W	10/06/00 11:11 PST	290.17 (4)		0.23	290.2	290.4* (0.1)	+0.2
Bridgeport grassland	38.2955N / 119.2693W	4/04/00 11:19 PST	306.2 (4)		(≈ 2.5)	306.2	303.7 (2.3)	-2.5
Bridgeport grassland	38.2202N / 119.2693W	7/25/00 11:18 PST	303.9 (2)		(≈ 2.5)	303.9	307.0 (1.1)	+3.1
Bridgeport grassland	38.2202N / 119.2693W	7/27/00 23:09 PST	281.33 (4)		(≈ 0.8)	281.3	281.8 (0.4)	+0.5
Bridgeport grassland	38.2202N / 119.2693W	7/29/00 22:57 PST	282.70 (4)		(≈ 0.8)	282.7	283.0 (0.2)	+0.3
rice field	39.5073N / 121.8107W	7/27/00 23:10 PST	291.29 (1)			291.3	291.8 (0.5)	+0.5
rice field	39.5073N / 121.8107W	7/29/00 22:57 PST	292.93 (1)			292.9	293.1 (0.8)	+0.2

* from L1B data in version 2.4.3

Figure 1

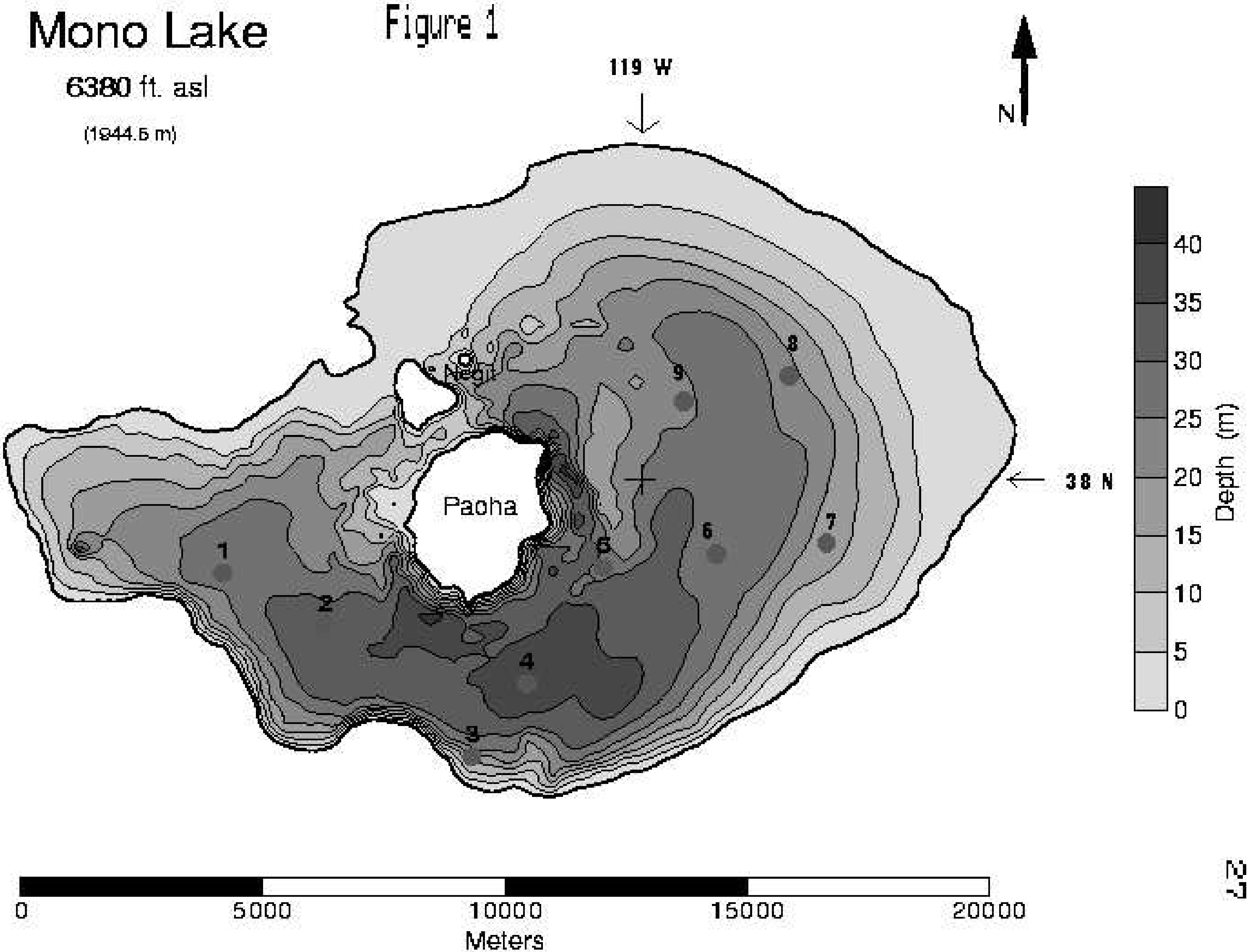
Mono Lake
6380 ft. asl
(1944.5 m)
119 W
38 N
N
Negit
Paoha
1
2
3
4
5
6
7
8
9
40
35
30
25
20
15
10
5
0
Depth (m)
0
5000
10000
15000
20000
Meters